frontiers in Molecular Biosciences

ORIGINAL RESEARCH
published: 15 March 2022
doi: 10.3389/fmolb.2022.849979

Structural Dissection of the First Events Following Membrane Binding of the Islet Amyloid Polypeptide

Lucie Khemtemourian[1], Hebah Fatafta[2,3], Benoit Davion[1], Sophie Lecomte[1], Sabine Castano[1] and Birgit Strodel[2,3,4]**

[1]Université de Bordeaux, CNRS, Bordeaux IMP, CBMN, Pessac, France, [2]Institute of Biological Information Processing, Structural Biochemistry, Jülich, Germany, [3]JuStruct, Jülich Center for Structural Biology, Jülich, Germany, [4]Institute of Theoretical and Computational Chemistry, Heinrich Heine University Düsseldorf, Düsseldorf, Germany

The islet amyloid polypeptide (IAPP) is the main constituent of the amyloid fibrils found in the pancreas of type 2 diabetes patients. The aggregation of IAPP is known to cause cell death, where the cell membrane plays a dual role: being a catalyst of IAPP aggregation and being the target of IAPP toxicity. Using ATR-FTIR spectroscopy, transmission electron microscopy, and molecular dynamics simulations we investigate the very first molecular steps following IAPP binding to a lipid membrane. In particular, we assess the combined effects of the charge state of amino-acid residue 18 and the IAPP-membrane interactions on the structures of monomeric and aggregated IAPP. Distinct IAPP-membrane interaction modes for the various IAPP variants are revealed. Membrane binding causes IAPP to fold into an amphipathic α-helix, which in the case of H18K-, and H18R-IAPP readily moves beyond the headgroup region. For all IAPP variants but H18E-IAPP, the membrane-bound helix is an intermediate on the way to amyloid aggregation, while H18E-IAPP remains in a stable helical conformation. The fibrillar aggregates of wild-type IAPP and H18K-IAPP are dominated by an antiparallel β-sheet conformation, while H18R- and H18A-IAPP exhibit both antiparallel and parallel β-sheets as well as amorphous aggregates. Our results emphasize the decisive role of residue 18 for the structure and membrane interaction of IAPP. This residue is thus a good therapeutic target for destabilizing membrane-bound IAPP fibrils to inhibit their toxic actions.

Keywords: islet amyloid polypeptide, type 2 diabetes mellitus, amylin, amyloid aggregation, peptide-membrane interactions

OPEN ACCESS

Edited by:
Javier Oroz, Spanish National Research Council (CSIC), Spain

Reviewed by:
Philippe Derreumaux, UPR9080 Laboratoire de Biochimie Théorique (LBT), France
Ling-Hsien Tu, National Taiwan Normal University, Taiwan

****Correspondence:***
Lucie Khemtemourian
lucie.khemtemourian@u-bordeaux.fr
Birgit Strodel
b.strodel@fz-juelich.de

Specialty section:
This article was submitted to Protein Folding, Misfolding and Degradation, a section of the journal Frontiers in Molecular Biosciences

Received: *06 January 2022*
Accepted: *18 February 2022*
Published: *15 March 2022*

Citation:
Khemtemourian L, Fatafta H, Davion B, Lecomte S, Castano S and Strodel B (2022) Structural Dissection of the First Events Following Membrane Binding of the Islet Amyloid Polypeptide. Front. Mol. Biosci. 9:849979. doi: 10.3389/fmolb.2022.849979

1 INTRODUCTION

The formation of amyloid fibrils is involved in various human diseases, such as Alzheimer's disease, Parkinson's disease, or type 2 diabetes mellitus (T2DM). Amyloid forming proteins are often intrinsically disordered proteins (IDPs) or are proteins that contain one or more intrinsically disordered regions. The structure of those amyloid fibrils are very heterogeneous but they are all composed of arrays of cross β-sheets (Selkoe, 2004; Knowles et al., 2014; Willbold et al., 2021).

The human islet amyloid polypeptide (hIAPP), also known as amylin, is a 37-amino acid peptide hormone that is the main constituent of the islet amyloid mainly found in the pancreatic islets of T2DM patients, but also in many organs including the brain, the heart, and the kidney (Westermark et al., 1987; Cooper et al., 1988; de Koning et al., 1995; Despa et al., 2012; Srodulski et al., 2014).

hIAPP is produced and secreted together with insulin by the pancreatic β-cells, and it plays a role in the control of glucose homeostasis and satiety by acting on the liver, gut, brain and pancreas (Lutz, 2010; Westermark et al., 2011). Under normal conditions, monomeric hIAPP lacks a well-defined structure as typical for an IDP, and mainly adopts a random coil conformation. However, in T2DM patients, hIAPP starts to aggregate into amyloid fibrils and the formation of these amyloid aggregates has been associated with the dysfunction and death of β-cells (Opie, 1901; Höppener et al., 2000).

While the toxic activity of hIAPP is still not completely understood, a link between hIAPP fibril formation at the membrane interface and hIAPP-induced cell death was observed, highlighting the relevance of the membrane (Gao and Winter 2015). A few putative mechanisms of cell membrane-disruption by hIAPP have been described and have been the subject of several studies (Mirzabekov et al., 1996; Janson et al., 1999; Engel et al., 2008; Hebda and Miranker, 2009; Martel et al., 2016). It has been suggested that the amyloid fibrils are not the primary toxic species, but oligomers formed by hIAPP are thought to be cytotoxic, either by forming membrane channels or by inducing bilayer disorder (Mirzabekov et al., 1996; Kayed et al., 2004; Quist et al., 2005). In agreement with these studies, molecular dynamics (MD) simulations demonstrated that membrane permeability was induced by oligomeric hIAPP (Poojari et al., 2013). Further experimental studies have indicated that the formation of hIAPP fibrils at the membrane causes membrane disruption by forcing the curvature of the bilayer to unfavorable angles or by the uptake of lipids by the fibrils (Sparr et al., 2004; Engel et al., 2008). Moreover, the composition of the membrane plays a role in the amount of membrane damage that can be caused by hIAPP (Zhang et al., 2017), and that by blocking hIAPP-membrane interactions by small-molecule ligands such as resveratrol, the membrane-induced toxicity of hIAPP can be alleviated (Evers et al., 2009). Even if the mechanism is not yet fully understood, altogether these studies revealed the importance of the membrane in hIAPP-induced cell death.

Along with these results, it has been recognized that the various amino acids of hIAPP are crucial in hIAPP fibril formation and in hIAPP-membrane disruption. The N-terminal residues are mainly responsible for membrane binding, the middle core drives amyloid fibril formation, while the C-terminal residues are also involved in amyloid fibril formation, yet to a lesser extent (Skeby et al., 2016; Engel et al., 2006; Brender et al., 2008a,b). The sequence of IAPP is highly conserved across different species (Cao et al., 2013; Caillon et al., 2016), however key differences, that play important roles in modulating the propensity of the peptide to aggregate, have been identified. The non-amyloidogenic, and non-toxic mouse IAPP differs from hIAPP by six residues out of 37; interestingly, five of the six residues are located in the amyloid-prone region 20–29 and mice do not develop T2DM. For that reason, it is essential to explore the sequence-structure relationship. While the region 20–29 is of relevance (Choi et al., 2021), it is not the sole region governing IAPP fibril formation, since proline mutations at positions 14, 15, 16, and or 17 can also induce a loss of fibril formation (Abedini and Raleigh, 2006; Fox et al., 2010; Tu and Raleigh, 2012). Recent studies on residue 18, that is highly variable among species (Caillon et al., 2016), indicate that this residue is important in modulating 1) IAPP fibril formation in solution and in the presence of membranes (Khemtemourian et al., 2017; Hoffmann et al., 2018a), 2) membrane interaction and damage (Hoffmann et al., 2018a), 3) cell toxicity (Khemtemourian et al., 2017), and 4) hIAPP-zinc, and hIAPP-insulin affinity (Wineman-Fisher and Miller, 2016; Khemtemourian et al., 2021; Miller, 2022). The main findings from these studies are summarized in **Table 1**.

The characterization of the aggregation pathways and of the structure at a molecular and an atomic level at the membrane is thus a key step to understanding hIAPP cellular toxicity and its role in disease states. While the structure of hIAPP in solution was extensively studied (Goldsbury et al., 2000; Williamson and Miranker, 2007; Wiltzius et al., 2009; Camargo et al., 2017), only a few studies were performed in a membrane environment. These studies mainly used spectroscopic techniques such as circular dichroism (CD) or nuclear magnetic resonance (NMR) spectroscopy (Jayasinghe and Langen, 2005; Patil et al., 2009; Nanga et al., 2011; Caillon et al., 2013; Camargo et al., 2017; Milardi et al., 2021), which yield information on structural averages of the conformational ensemble, yet are not time-resolved enough to provide information on individual structures. A complicating aspect for NMR spectroscopy of hIAPP in the presence of lipid bilayers is the fast aggregation speed of hIAPP. To overcome this challenge, approaches have been adopted to reduce the fibrillation process, such as the use of low temperatures and/or detergent micelles that stabilize the monomeric form of hIAPP (Jayasinghe and Langen, 2005; Patil et al., 2009; Nanga et al., 2011; Caillon et al., 2013; Camargo et al., 2017). Here, we address this problem by employing a combination of two techniques that offer the possibility of obtaining time-resolved structural information of hIAPP in a membrane environment, namely attenuated total reflection Fourier-transform infrared (FTIR) spectroscopy and MD simulations. This allows us to provide structural information for both monomeric hIAPP as well as the first aggregation steps of hIAPP at the membrane. Previous simulation studies examined the membrane interactions of monomeric and oligomeric hIAPP (Martel et al., 2016; Dignon et al., 2017a; Dong et al., 2018; Press-Sandler and Miller, 2018; Qian et al., 2018; Qiao et al., 2019). The results from these simulations indicate that wild-type hIAPP interacts with the membrane by forming interactions between the anionic lipids of the membrane and the N-terminal part of hIAPP, which is in agreement with experimental data (Engel et al., 2006; Skeby et al., 2016). Stabilization of the α-helical state following the binding to a membrane was also observed in both experimental and simulation studies (Caillon et al., 2013; Dignon et al., 2017a; Christensen et al., 2021). FTIR spectroscopy has been previously used to provide insights into the membrane-bound monomeric and fibril structures of hIAPP (Mishra et al., 2008; Mishra and Winter 2008; Radovan et al., 2008). The studies indicated that a transition from unordered structures to β-sheet structures occurs on a time scale characteristic for amyloid fibril formation. Possible structures for membrane-bound hIAPP

TABLE 1 | Biophysical and biological characteristics of wild-type and mutated hIAPP as determined in previous studies.

	hIAPP	H18R-IAPP	H18K-IAPP	H18E-IAPP	H18A-IAPP
Fibril formation in solution	+++	++	+	+	+
Fibril formation at membranes	+++	+++	++	+	+
Membrane leakage	+++	+++	+++	+++	+++
Cell toxicity	+++	+	+	+	+

aggregates were suggested by MD simulations (Liu et al., 2020; Nguyen et al., 2021; Sepehri et al., 2021).

The purpose of this study is to reveal the structures of hIAPP directly after its binding to a lipid-membrane interface and to determine how these structures are influenced by histidine 18. To this end, both experiments and simulations were performed as they provide information on the structural evolution for different length and time scales and with different resolutions, thereby complementing each other. To study the effects of residue 18 on the hIAPP-membrane interactions and the emerging peptide structures, all the experiments and simulations were performed with wild-type hIAPP and four mutated peptides where histidine 18 has been replaced by arginine (H18R-IAPP), lysine (H18K-IAPP), glutamic acid (H18E-IAPP), and alanine (H18A-IAPP) to achieve variations in charge, shape, volume, and hydrophobicity. To evaluate the interaction of hIAPP and the mutated peptides with the membrane, we worked with a 1, 2-dioleoyl-sn-glycero-3-phosphocholine/1,2-dioleoyl-sn-glycero-3-phospho-L-serine (DOPC/DOPS) lipid mixture (ratio 7:3) to mimic eukaryotic β-cell membranes. These cells contain typically between 1 and 10% of negatively charged lipids; however in the case of T2DM, the high concentration of glucose increases the amount of negatively charged lipids up to 30% (Rustenbeck et al., 1994). We performed attenuated total reflection (ATR) FTIR spectroscopy at different incubation times to apprehend the initial structure of the peptides at the membrane and the evolution of structural changes. The putative perturbation of the lipid membranes after addition of the peptides was also investigated. We observed differences for the wild-type and the mutated peptides not only in the initial structures but also in the variation of secondary structure in time, highlighting the role of the residue histidine 18 in the membrane interactions of hIAPP and in the process of fibril formation. The ATR-FTIR results are complemented on either side of the length and time scales, by MD simulations to provide mechanistic insight into the structural transitions and peptide-membrane interactions and by transmission electron microscopy (TEM) to obtain images of the final fibrils.

2 MATERIALS AND METHODS

2.1 Sample Preparation

Peptide solutions were prepared as described previously (Khemtemourian et al., 2017; Hoffmann et al., 2018a). Briefly, stock solutions were obtained by dissolving the peptide powder at a concentration of 1 mM in hexafluoroisopropanol (HFIP) and by letting them incubate for an hour. HFIP was then evaporated under a stream of dry N_2 and further dried by vacuum in a desiccator for at least 30 min. The resulting peptide film was then rehydrated with 100 μl of buffer containing 10 mM tris(hydroxymethyl)aminomethane and 100 mM NaCl (pH 7.4) and 2 μL of a 20 μM $CaCl_2$ solution.

2.2 Preparation of Phospholipid Vesicles

DOPC and DOPS lipids were purchased from Avanti Polar Lipids. Lipid powders were dissolved in chloroform and mixed at the desired ratio. The solvent was evaporated under a stream of dry nitrogen and further dried under high vacuum in a desiccator for at least 30 min. Lipid films were then rehydrated for 1 h with a buffer of 10 mM Tris, 100 mM NaCl, pH 7.4 in 100% D_2O, obtaining large, and multilamellar vesicles (LMVs). Small, unilamellar vesicles (SUVs) were then prepared from the LMVs by tip sonication. The SUVs were burst onto a germanium ATR crystal to form a single bilayer which is controlled by the measurement of the absolute IR intensity. For the subsequent measurements, we added hIAPP (or its mutants) at 50 μM concentration to the membrane and then rinsed the non-binding peptides off.

Large, unilamellar vesicles (LUVs) for the TEM were prepared using the same buffer conditions as for the LMVs, but containing 100% H_2O, which was subjected to 10 freeze-thaw cycles with alternating temperatures of about −190°C and 50°C. The lipid suspension was subsequently extruded 19 times through a mini-extruder (Avanti Polar Lipids) equipped with a 200 nm polycarbonate membrane. The phospholipid content of both lipid stock solutions and vesicles was determined as inorganic phosphate according to Rouser et al. (Rouser et al., 1970).

2.3 ATR-FTIR Spectroscopy

ATR-FTIR spectra were recorded on a Nicolet 6,700 spectrometer Thermo Scientific equipped with an MCT detector cooled at 77 K. A Ge-crystal was used as internal reflection unit. Since ATR-FTIR spectroscopy is sensitive to the orientation of the structures (Goormaghtigh et al., 1990; Goormaghtigh et al., 1994; Goormaghtigh et al., 1999), spectra were recorded with parallel (p) and perpendicular (s) polarizations of the incident light with respect to the ATR plate. 200 scans were recorded at a resolution of 8 cm^{-1}. All the orientation information is then contained in the dichroic ratio $R_{ATR} = A_p/A_s$, where A_p and A_s represent the absorbance underlying the band at p and s, respectively, polarization of the incident light. After subtraction of a spectrum of the lipid membrane with the buffer and subtraction of noise from water, the spectra were baseline-corrected between 1700 and 1,600 cm^{-1} corresponding to the amide I band area. Finally, a smoothing has been applied. To derive the secondary structure from the bands, the spectra were

analyzed with an algorithm based on a second-derivative function and a self-deconvolution procedure (GRAMS and OMNIC software, Thermo Fisher Scientific) to determine the number and wavenumber of the individual bands within the spectral range of the amide I band.

2.4 Transmission Electron Microscopy

TEM was performed at the "Institut de Biologie Paris Seine" (IBPS, Sorbonne Université, Paris, France). Peptides and LUVs were incubated for 2 days at room temperature. Aliquots (20 μl) were adsorbed onto a glow-discharged carbon coated 200 mesh copper grid for 2 min and then negatively stained with saturated uranyl acetate for 45 s. Grids were examined using a ZEISS 912 Ω electron microscope operating at 80 kV.

2.5 Computational Methods

2.5.1 Setup of the Simulated Systems

The modeled systems are composed of the full-length (37 residues) hIAPP monomer (either wild-type or mutated at residue 18) and a DOPC/DOPS lipid bilayer in a 7:3 ratio mimicking the lipid composition of the experiments. As initial peptide structure, the most populated conformation from a preceding 1 μs simulation of wild-type hIAPP as a monomer and with a disulfide bond between C2 and C7 in the aqueous phase was used. The mutated peptides were generated from this structure by replacing the neutral H18 residue (protonated only at Nϵ) by its positively charged counterpart (denoted by H18+), the neutral residue alanine, the negatively charged glutamate, or the positively charged lysine or arginine using the CHARMM-GUI interface (Lee et al., 2016). These peptides will be referred to as hIAPP, hIAPP(H18+), H18A-IAPP, H18E-IAPP, H18K-IAPP, and H18R-IAPP, respectively. CHARMM-GUI was also used to set up and equilibrate the DOPC/DOPS lipid bilayer as a symmetric membrane composed of 88 DOPC and 40 DOPS lipid molecules. The peptides were placed above the lipid bilayer (one peptide per simulation) at a distance of ≈3 nm from the bilayer surface. Each system was then solvated with water using the TIP3P model (Jorgensen et al., 1983) and NaCl was added at physiological concentration of 150 mM, while also neutralizing the system. The total number of atoms N in each system was ≈54,000 atoms and the simulation box size was about $6.5 \times 6.5 \times 12.0$ nm^3.

2.5.2 MD Simulation Conditions

The MD simulations were carried out using the GROMACS 2018.2 simulation package (Abraham et al., 2015), along with CHARMM36 (Klauda et al., 2010) as force field for the lipids and CHARMM36m (Huang et al., 2017) for the IAPP peptides. Each system was first energy minimized using the steepest descent algorithm to remove initial atom clashes that may have resulted during the setup. This was followed by an equilibration using MD simulations under *NVT* conditions, where the reference temperature T of 302 K (which was chosen to be close to the temperatures used in the experiments) was regulated with a velocity-rescale thermostat (Bussi et al., 2007). Then, the system was equilibrated under *NpT* conditions to obtain a pressure p of 1.0 bar, which was realized by regulating the pressure using a semi-isotropic Parrinello-Rahman pressure coupling scheme (Berendsen et al., 1984). The particle mesh Ewald (PME) method was used to calculate the electrostatic interactions in combination with periodic boundary conditions set in all directions. The electrostatic interactions in real space as well as the van der Waals interactions were cut at 1.2 nm. All bonds were constrained using the LINCS algorithm (Hess et al., 1997). For each of the six systems the MD simulations were run in triplicate and for 1 μs per simulation (i.e., 3×1 μs per system).

2.5.3 Analysis of the MD Simulations

All analysis programs mentioned are available via the GROMACS 2018.2 program package (Abraham et al., 2015). Only the MD snapshots were IAPP is within 0.5 nm of the bilayer were included in the analysis of the system in question. The peptide-lipid interactions were then determined by calculating the interaction energy between each IAPP residue and the DOPC and DOPS lipids, respectively, using "gmx energy". The "gmx mindist" program was employed to determine the number of contacts between each IAPP residue and DOPC/DOPS. A contact was recorded when the distance between any two non-hydrogen atoms from a residue and a lipid was within 0.5 nm. The hydrogen bond propensity was determined as the ratio of the number of MD snapshots where one or more hydrogen bonds were formed between peptide and lipid and the total number of MD snapshots per system. The secondary structure of the peptides was determined using the 'define secondary structure program' (DSSP) (Kabsch and Sander, 1983) invoked via the GROMACS tool "do dssp". To facilitate a clear representation, the data of similar secondary structures are grouped together: β-strand and β-bridge are combined as β-sheet, β-turn and bend as turn, and helix includes α-, π-, and 3_{10}-helices.

3 RESULTS

3.1 hIAPP and the Mutated Peptides Adopt a Mixture of Structures Upon Initial Binding to the Membrane

We first investigated, using ATR-FTIR spectroscopy, the structural behavior of wild-type and mutant hIAPP when interacting with a (supported) lipid bilayer composed of DOPC/DOPS (7:3). These phospholipids represent the most abundant zwitterionic phospholipid species (PC) and the dominant negatively charged phospholipid species (PS) in eukaryotic cells, and the 7:3 ratio is similar to the one of zwitterionic lipids to negatively charged lipids of the membrane of pancreatic islet cells (Rustenbeck et al., 1994). We performed polarized ATR-FTIR experiments in order to analyze the initial structures of the peptides at the membrane and to determine if the mutation at residue 18 could induce some structural changes. **Figure 1** shows the ATR-FTIR spectra in the amide I region of hIAPP and the mutated peptides interacting with DOPC/DOPS bilayers. Based on the amide I band analysis, hIAPP and H18K-IAPP exhibit two peaks at around 1643 ±

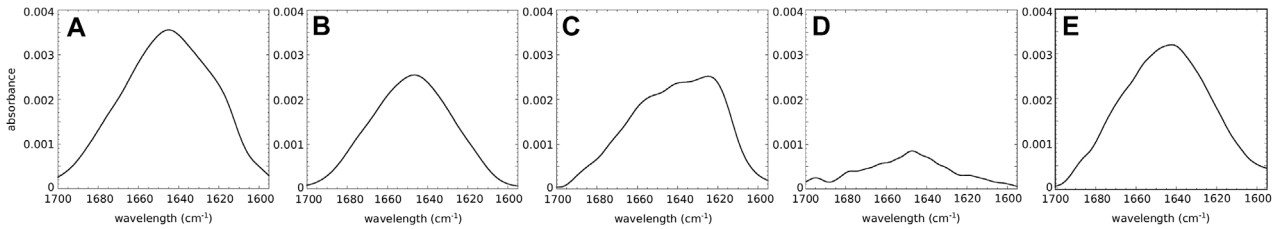

FIGURE 1 | ATR-FTIR spectra for the amide I range of **(A)** hIAPP and the mutated peptides **(B)** H18R-IAPP, **(C)** H18K-IAPP, **(D)** H18E-IAPP, and **(E)** H18A-IAPP interacting with a lipid bilayer composed of DOPC/DOPS (7:3).

TABLE 2 | Secondary structure content derived from ATR-FTIR spectra of hIAPP and its mutants interacting with a DOPC/DOPS membranes.

Secondary structure element	Wavenumber (cm^{-1})	Percentage of structural elemnt				
		hIAPP	H18R-IAPP	H18K-IAPP	H18E-IAPP	H18A-IAPP
β-sheet (‖ and anti-‖)	1615, 1624, 1632, 1686	31	27	36	23	34
Random coil	1643	40	41	37	49	34
α-helix	1654	18	19	19	12	20
Turn	1674	11	13	8	16	12

1 cm^{-1} and 1623 ± 1 cm^{-1} assigned to random coil and β-sheet structure, respectively. The mutated peptides H18R-IAPP, H18E-IAPP, and H18A-IAPP display predominantly an amide I band at around 1643 ± 1 cm^{-1} that can be attributed to unordered secondary structures. The secondary structure content of the peptides bound to the DOPC/DOPS bilayers has then been evaluated from the analysis of the amide I band shape and curve fitting (**Table 2**). The bands at 1686 ± 1 cm^{-1}, 1632 ± 1 $cm1^{-1}$, 1624 ± 1 cm^{-1}, and 1615 ± 1 cm^{-1} were assigned to β-sheets (parallel and antiparallel), the band at 1654 ± 1 cm^{-1} to α-helices, the band at 1643 ± 1 cm^{-1} to random structures, and the one at 1674 ± 1 cm^{-1} to β-turns. The results show that hIAPP is mainly unstructured (40%) with a contribution of β-sheets (31%), which is in agreement with previous studies (Khemtémourian et al., 2010; Seeliger et al., 2012). The peptides H18R-IAPP and H18K-IAPP adopt unstructured conformations with about the same probability as hIAPP (41 and 37%, respectively) but have different amounts of β-sheets (27 and 36%). The initial structure of H18E-IAPP differs substantially from the wild-type peptide with less β-sheet content and more random coil conformation. The peptide H18A-IAPP has the highest content of α-helical structure and the lowest amount of random coil, which is likely due to the inherent preference of alanine to adopt a helical conformation; in fact, alanine is regarded as the most stabilizing residue in helices. Such change in the initial structure may modify the kinetics of fibril formation as shown previously (Hoffmann et al., 2018a). Overall, the data indicate that at the membrane interface, hIAPP is initially largely unstructured, but depending on the kind of mutation at residue position 18, the peptides also adopt β-sheet, and α-helical structures to different extents. In order to determine if these mutations do also influence the kinetics of structural changes, the ATR-FTIR experiments were carried out during the course of a few hours.

3.2 Residue 18 is Decisive for the Conformational Rearrangements of Membrane-Bound IAPP

To evaluate the changes in secondary structure of the IAPP peptides at the DOPC/DOPS membrane interface, we collected ATR-FTIR spectra for 2 h in intervals of 30 min. **Figure 2A** shows that the maximum of the amide I band of hIAPP undergoes a pronounced shift from 1643 cm^{-1} to 1624 cm^{-1}. This shift corresponds to a structural transition from an unstructured conformation to a structured one with antiparallel β-sheets, indicating the start of the peptide aggregation process. The maximum at 1624 cm^{-1} is reached at 120 min. However, a shoulder at around 1650 cm^{-1} remains, for which there are two possible explanations: 1) not all of the amino acids are involved in the intermolecular β-sheet formation, or 2) monomers and/or oligomers are still present after 2 h of incubation. In two previous studies, we observed that the monomeric hIAPP is fully consumed within 2 h and that low-molecular weight hIAPP oligomers were not detected Hoffmann et al. (2018a,b). doi: 10.1039/c7cp07516b.) The first explanation is thus the more probable. The secondary structure content of the membrane-bound hIAPP at different incubation times (from 0 to 120 min) resulting from the analysis of the amide I band shape and curve fitting is given in **Figure 2B**. The bar chart clearly indicates that the β-sheet content increased from 31 to 50%, while the random coil content decreased from 37 to 26%, meaning that hIAPP started to aggregate, in agreement with previous studies (Mishra et al., 2008). Nonetheless, some of the residues remained in an α-helical conformation, as this contribution dropped to ony about 15%, starting from 18% at time zero.

The same kind of experiments were performed for the mutated peptides. While they all undergo structural rearrangements, different behaviors are observed. As for hIAPP, the antiparallel

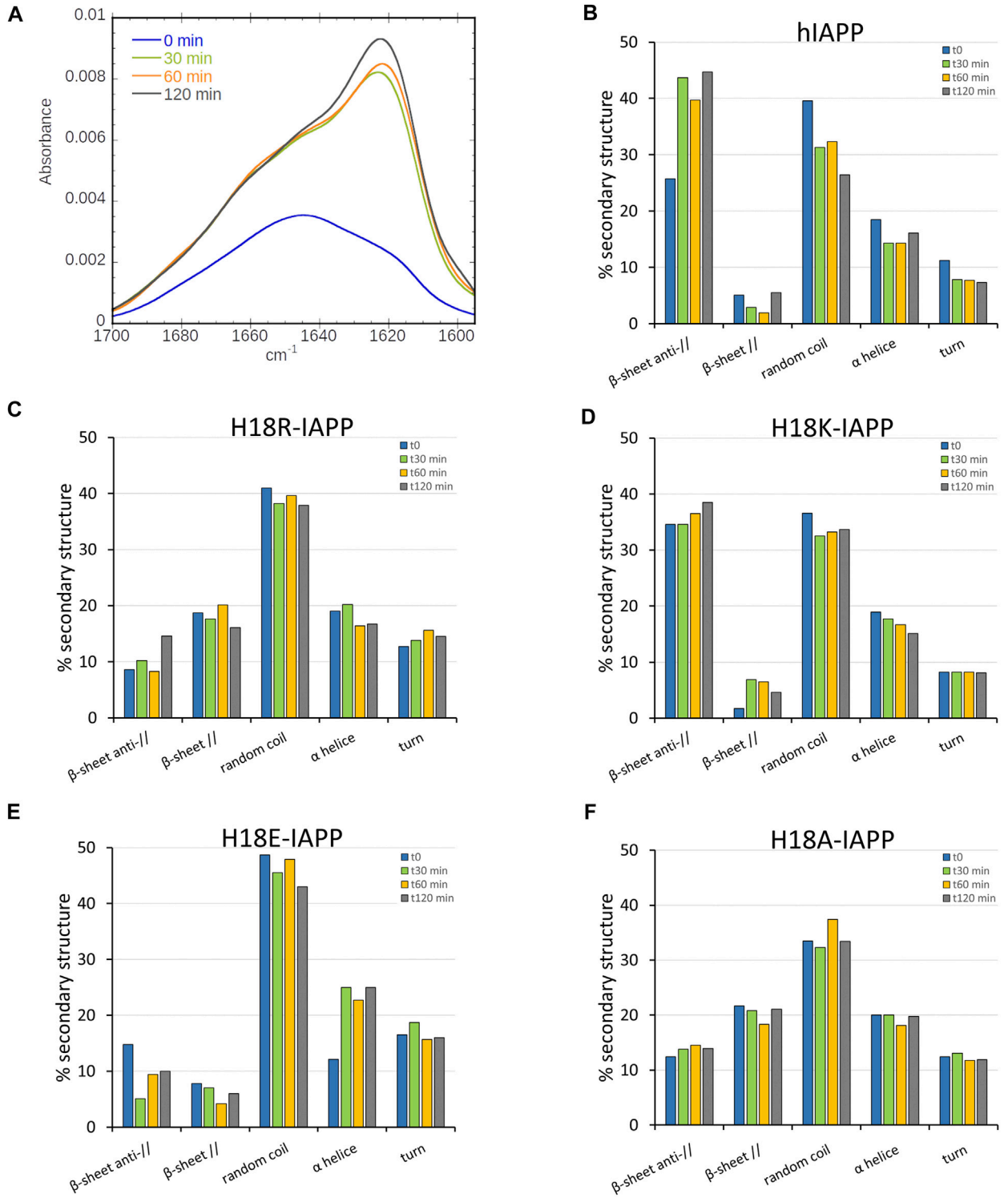

FIGURE 2 | (A) Time-evolution (from 0 min, black, to 120 min, and red) of the ATR-FTIR spectra of hIAPP. Secondary structure analysis for **(B)** hIAPP and the mutated peptides **(C)** H18R-IAPP, **(D)** H18K-IAPP, **(E)** H18E-IAPP, and **(F)** H18A-IAPP. The bars show the averaged content of secondary structures including antiparallel and parallel β-sheets, random coil, α-helices, and turns.

β-sheet content of H18K-IAPP increases over time, thereby reducing the amount of random coil conformations, which suggests a self-assembly of the peptide (**Figure 2D**). It should be noted that already the structure of H18K-IAPP at the beginning of the experiment contains considerable amounts of antiparallel β-sheet, indicating that the aggregation of this peptide

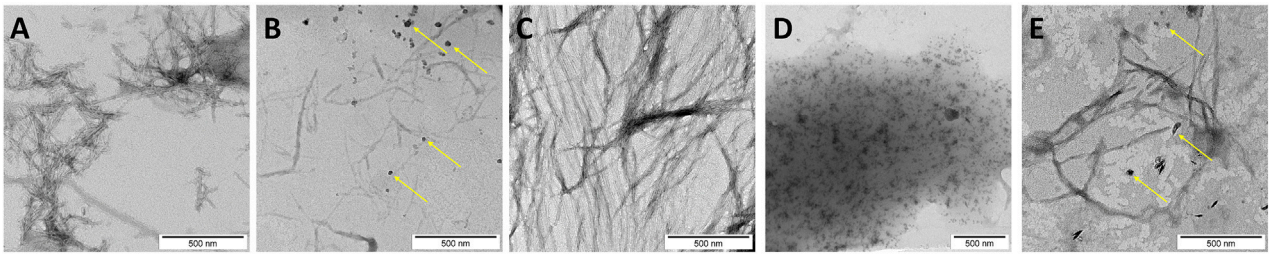

FIGURE 3 | TEM image of **(A)** native hIAPP and the mutated peptides: **(B)** H18R-IAPP, **(C)** H18K-IAPP, **(D)** H18E-IAPP, and **(E)** H18A-IAPP incubated with DOPC/DOPS liposomes. The yellow arrows indicate the amorphous aggregates found for H18R-IAPP and H18A-IAPP. Scale bars represent 500 nm.

is immediate. Also in the cases of H18R-IAPP and H18A-IAPP there are β-sheets present at $t = 0$, yet they include both parallel and antiparallel arrangements, suggesting the presence of two structural populations (**Figures 2C,F**). These two populations are largely stable over time; only for H18R-IAPP some increase in antiparallel β-sheet content is observed at $t = 120$ min. In the case of H18E-IAPP, on the other hand, the amount of both parallel and antiparallel β-sheet decreases, whereas α-helical structures are increasingly formed (**Figure 2E**), reaching helical contents of more than 20%. This suggests that the DOPC/DOPS membrane promotes an α-helical conformation in membrane-bound H18E-IAPP. It should be mentioned that also in the case of H18A-IAPP the initial α-helix that formed remained stable, with population values of about 20%, whereas in H18K-IAPP and H18R-IAPP the helical content decreased somewhat to about 15%, which is similar as for hIAPP. In order to corroborate these results and validate the presence of one or two β-sheet populations, we then performed TEM in the presence of DOPC/DOPS membranes.

3.3 Electron Microscopy Images Validate the Structural Differences Between the Peptides

TEM was applied to assess the presence of amyloid fibrils and/or amorphous aggregates interacting with the membrane. In the case of hIAPP, fibrils were obtained that exhibit a classical and mature amyloid-fibril morphology with widths of 6–10 nm (**Figure 3A**). It seems reasonable to assign these fibrils to the antiparallel β-sheets structure observed in the ATR-FTIR experiments. The same result is found for H18K-IAPP, where long and twisted fibrils are observed by TEM (**Figure 3C**), and which mainly harbor antiparallel β-sheets as revealed by the ATR-FTIR spectrum. For H8R-IAPP and H18A-IAPP, two aggregate morphologies are present in the TEM images, one corresponding to short fibrils, and the other one being small amorphous aggregates (indicated by yellow arrows in **Figures 3B,E**). These results correlate with the ATR-FTIR experiments of both peptide variants that display two β-sheet populations: parallel and antiparallel β-sheets. Based on the observation that in the cases of hIAPP and H18K-IAPP the fibrils are correlated with the appearance of antiparallel β-sheets, we assume that also for H18R-IAPP and H18A-IAPP the antiparallel β-sheets give rise to fibrils, and while the parallel β-sheets are most likely present in the amorphous aggregates. This suggests that amorphous aggregates and fibrils can not only be distinguished from each other, but they also arise from different secondary and tertiary structures. For H18E-IAPP, no fibrils were detected in the TEM images, only small aggregates occurred (**Figure 3D**). The β-sheet content (both parallel and antiparallel) was also low; instead, the amount of random coil is rather high, suggesting that the amorphous H18E-IAPP aggregates are mainly unstructured while involving some helices. The current findings correlate with previous results that the substitution of the histidine 18 by an arginine, an alanine, or a glutamate stabilizes the oligomeric species and slows down the fibril formation (Hoffmann et al., 2018a). To gain more insights into the impact of residue 18 on the initial structure of the peptides and on the membrane interactions of IAPP and resulting structural changes, we performed all-atom MD simulations.

3.4 MD Simulations Provide Atomic Insight Into the Different Behaviors of the Membrane-Bound IAPP Peptides

In order to elucidate the structure of membrane-bound hIAPP in its monomeric form, which cannot be captured by experimental means as it is in equilibrium with aggregated peptide species at the temporal resolutions of the experimental techniques, we performed MD simulations. Moreover, to unravel the effects of residue 18 on the peptide-membrane interactions and their joint consequences on the peptide structure, we simulated hIAPP (with neutral H18 and positively charged H18, denoted as H18+) and its mutants H18A, H18E, H18R, and H18K. For each peptide variant, we performed 3×1 μs MD simulations studying the binding of the peptides to a DOPC/DOPS (7:3) lipid bilayer.

3.4.1 Membrane Adsorption

To follow the association of the peptide with the membrane, we calculated the average distance between the center of mass of each residue and the average position along the bilayer normal of the phosphorus atoms of DOPC, which was used as a reference, and therefore set to zero (**Figure 4**). It can be seen that the peptides interact differently with the membrane. Similar distance profiles are observed for hIAPP, hIAPP(H18+), H18R-IAPP, and H18K-IAPP, while those of H18E-IAPP and H18A-IAPP are similar with

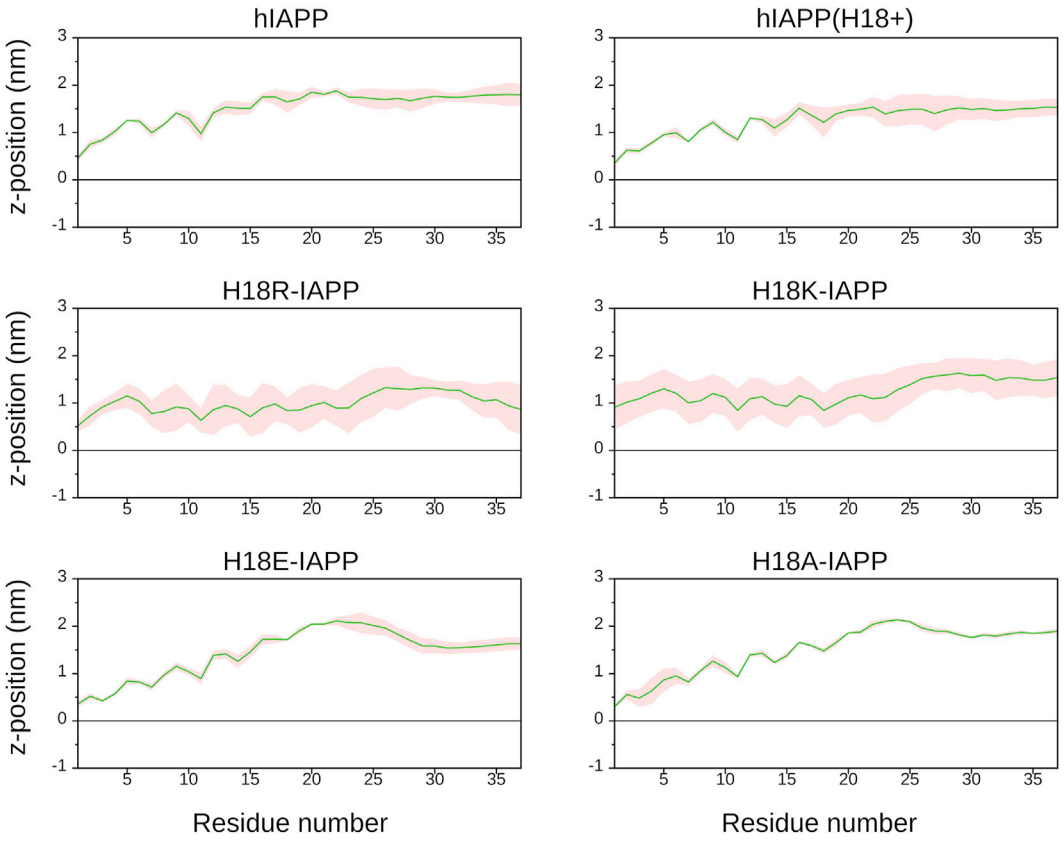

FIGURE 4 | The average distance (and standard error, shown as shaded area) between each IAPP residue and the DOPC/DOPS membrane surface, which is defined by the average *z*-position of the P atoms of DOPC (shown as black line).

each other yet differ from the other four. The smallest distances are witnessed for H18R-IAPP and H18K-IAPP, followed by hIAPP(H18+), which indicates that a positive charge at position 18 is key for its interaction with the membrane. The peptides generally approach the membrane with their N-terminus, with close contacts being formed between region K1–R19 and the lipids, while residues S20–Y37 are further away from the membrane. However, this does not apply to H18K-IAPP and H18R-IAPP, where almost all residues are within ≈1.0 nm of the membrane surface. In particular in the latter case, also the C-terminus is close to the membrane, indicating a parallel alignment of the peptide to the membrane surface, and which is not as strongly visible for the other peptides. The profiles of the distance plots are characterized by a zigzag pattern, which suggests that the peptides adopt a helical structure on the membrane, and that especially involves the first half of the peptides.

Figure 5 shows representative snapshots for the membrane association of IAPP, which confirms that the peptides tend to adopt a helical conformation in the N-terminal half. However, the wild-type peptides hIAPP and hIAPP(H18+) also involve a β-sheet in the C-terminal region (S20–G33), which was not adopted by the other peptides. In agreement to the distance plot one can see that hIAPP(H18+) inserts more deeply into the membrane than hIAPP, while hIAPP is only on, but not in the membrane. Nonetheless, in both cases the β-sheet interacts with the membrane, suggesting it to play a role in the subsequent aggregation when several peptides are membrane-adsorbed. These structures could even represent the α-to-β intermediate that was suggested to exist along the amyloid aggregation pathway of hIAPP, especially when this aggregation is assisted by the presence of lipid membranes (Abedini and Raleigh, 2009; Ling et al., 2009). Peptides H18R- and H18K-IAPP are seen to be immersed in the membrane. The helix, which reaches from T6 to G24 in both cases, lies below the lipid headgroup, and is parallel to the membrane surface. In the case of H18R-IAPP, also the C-terminal residues are close to the headgroups, whereas the C-terminus of H18K-IAPP points away from the membrane surface, which explains the slight difference in their distance profiles shown in **Figure 4**. In the case of H18E-IAPP, the helix is least developed and all residues that are not part of the helix point away from the membrane. With the H18A mutation, on the other hand, a helix is formed, and which however is not membrane-adsorbed. Only a few residues from the N- and C-terminal region make contact with the membrane, whereas the helix is several Angstrom above the membrane surface. The observation of a well-developed helix for H18A-IAPP is in line with the experimental findings and derives from the helix-promoting alanine introduced into the sequence. There are furter findings from the simulations that agree with the experimental

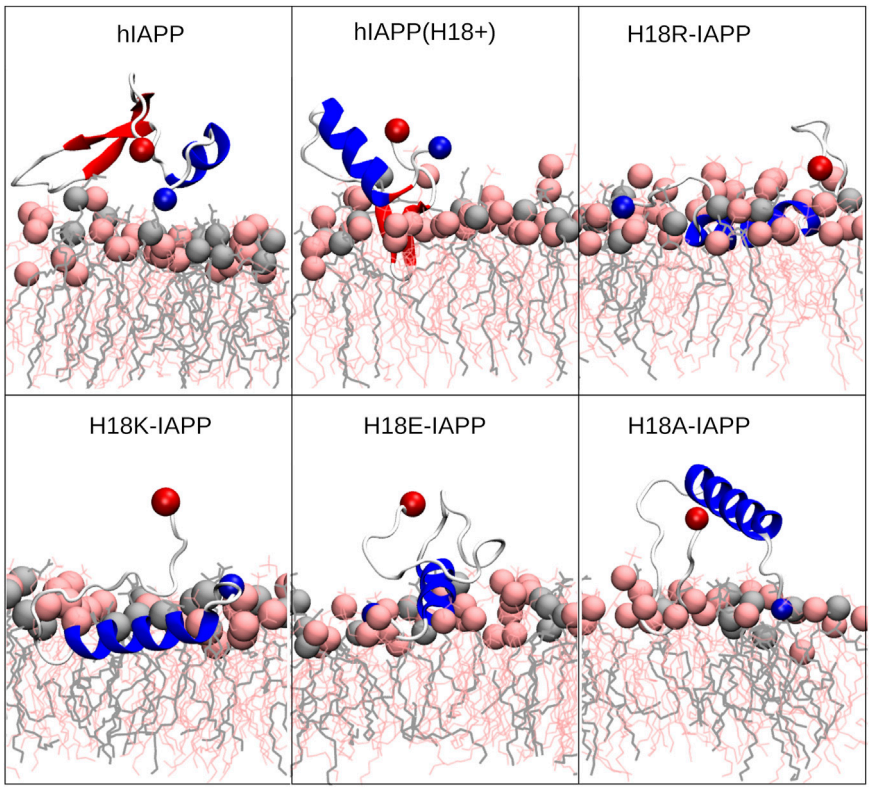

FIGURE 5 | Representative IAPP structures interacting with the DOPC/DOPS membrane. The peptide is shown as cartoon (with helix, β-sheet and coil being shown in blue, red and white, respectively), with their N- and C-termini being indicated as blue and red spheres, respectively. DOPC and DOPS lipids are shown as pink and gray sticks, respectively, with their P atoms indicated by spheres of the corresponding color.

results in **Table 2**. For instance, both simulations and experiments found that the α-helical content is smallest and that of random coil is largest for H18E-IAPP.

3.4.2 Secondary Structure

To quantify the effect of the peptide mutation and membrane adsorption on the peptide secondary structure, we determined the propensity of each peptide to adopt a helical conformation, to be part of a β-sheet (β-strand or β-bridge), or be in a turn or bend conformation. **Figure 6** shows that random coil and α-helices are the dominating structures, with probabilities between 30 and 40%, or even above. Turn conformations are populated with a probability of 20–25%, while the β-sheet content is $<1\%$, apart for hIAPP where it is $\approx 5\%$. All of the mutants have a higher amount of helix than hIAPP. For H18K-IAPP it even reaches 45%, which correlates with its close interaction with the membrane. However, while for H18R-IAPP the interaction with the membrane is similar, the increase in helix is not as pronounced (35%). The second highest amount in helix is observed for H18A-IAPP (38%), which agrees to the increase in helical propensity seen for this mutant in experiment (**Table 2**). Nonetheless, there are also certain differences between the secondary structures determined by the ATR-FTIR experiments and by the simulations, which can be explained with the different lenth, and time scales that are probed by these techniques. In the MD simulations, we model the very first peptide–membrane interaction of the IAPP monomer, whereas with the ATR-FTIR experiments the structural evolution occurring at later times can be assessed. However, at the time when the first ATR-FTIR spectrum is recorded, there are already small IAPP oligomers present in addition to monomers. The application of simulations besides ATR-FTIR spectroscopy therefore allows to extract the characteristics of the IAPP monomers which are hidden in spectroscopic signals of the monomer-oligomer mixtures. The presence of monomers only in the simulations explains the generally low amount of β-sheet that is present in the simulated systems, as this is expected to increase upon IAPP aggregation. Only for hIAPP, an average β-sheet content of 5% is observed that results from an intrapeptide β-hairpin that formed towards the end of the simulation. For hIAPP(H18+) it formed even later, therefore the average β-sheet content is lower, even though for this system a β-hairpin is clearly visible in **Figure 5**.

3.4.3 Peptide–membrane Interactions

To rationalize the driving force for IAPP to interact with the DOPC/DOPS lipid bilayer, the interaction energy of each peptide residue with each component of the lipid bilayer was calculated and partitioned into its electrostatic (E_{Coul}) and Lennard-Jones

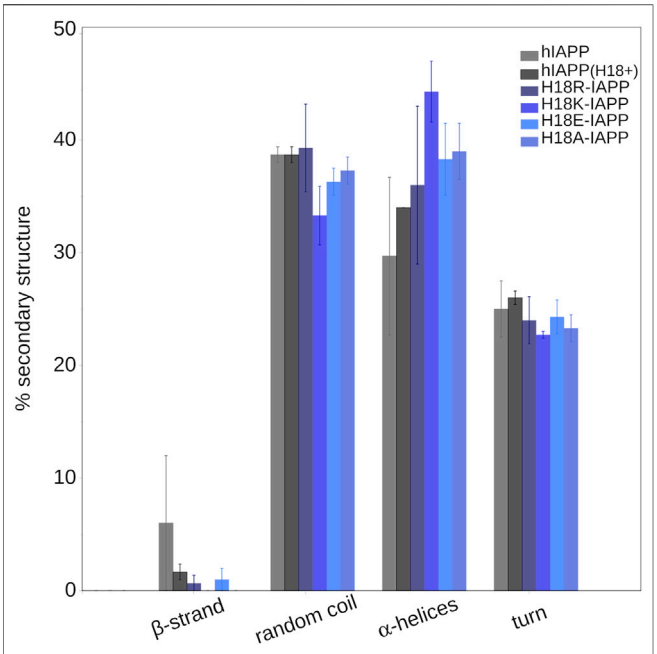

FIGURE 6 | The average secondary structure content (and standard error) in IAPP in the presence of a DOPC/DOPS membrane as obtained from MD simulations.

(E_{LJ}) contributions (**Supplementary Figure S1**). The results show that the major driving force for the peptide–membrane association are electrostatic attractions, especially between the negatively charged DOPS lipids, and the positively charged residues K1 and R11. These interactions occur in all cases and explain why IAPP approaches the membrane always via its N-terminus. This observation agrees with those from previous MD studies that highlighted the importance of anionic lipids like POPG (1-palmitoyl-2-oleoyl-sn-glycero-3-phosphoglycerol), POPE (1-palmitoyl-2-oleoyl-sn-glycero-3-phosphoethanolamine), and or DOPS in driving hIAPP–membrane interactions (Zhang et al., 2012; Dignon et al., 2017b; Mei et al., 2020). **Supplementary Figure S2** reveals that a positive charge at position 18 generally increases the tendency of the peptide to interact with the membrane. Almost all residues of the three peptides hIAPP(H18+), H18R- and H18K-IAPP form contacts with the membrane, whereas these contacts are mainly limited to K1–R11 in the other three cases. In the cases of H18R- and H18K-IAPP, the interaction between the positive charge of residue 18 and DOPS particularly enhances the association of the peptide with the membrane, which explains their deeper insertion into the membrane. This suggests that the size and/or flexibility of the side chain is important too. The electrostatic interactions partly involve H-bond formation in the region K1–R11, which extends to the C-terminal residues for hIAPP(H18+), and H18R- and H18K-IAPP (**Supplementary Figure S3**). Again, the positively charged residues are most involved in H-bond formation. The propensity of residue 18 to form an H-bond with DOPS or DOPC is particularly pronounced for H18R-IAPP, which is accompanied by further H-bonds between C-terminal residues and especially DOPC. Interestingly, in the experiments this peptide appeared to form fewer fibrils and more amorphous aggregates compared to hIAPP and H18K-IAPP. Its tendency to form H-bonds with the lipids may explain why H18R-IAPP has a reduced propensity to form fibrils, which requires H-bonds to be formed between the peptides in order to enable β-sheet formation.

3.4.4 Membrane Insertion Pathways

All-atom MD simulations allow to unravel the steps leading to the different peptide–membrane interactions in detail. An important aspect here is the high amount of hydrophobic residues present in IAPP, which give rise to an amphipathic helix when residues Q10 to L27 adopt an α-helix (**Figure 7A**). When such a helix binds to a membrane, it orients itself parallel to the membrane surface, with the hydrophobic side of this helix inserting into the hydrophobic core of the membrane, and the hydrophilic residues of the other side interacting with the lipid headgroups or the aqueous solvent (Christensen et al., 2021). This situation is visible for H18R-IAPP (**Figure 7B**). However, as the helix formed in this peptide only extends to S19, residues F23, I26 and L27 are not inserted into the membrane. **Figure 7B** further shows that the initial binding to the membrane is clearly driven by electrostatic interactions between the N-terminus and K1, which is followed by membrane insertion of the hydrophobic side of the amphipathic helix. This binding pattern is stabilized by interactions between R18 and the lipid headgroups, which is facilitated due to the length and flexibility of this side chain. For H18K-IAPP, the situation is similar, whereas in the case of hIAPP(H18+) the side chain is too short to enable strong interactions with the lipid headgroups. **Figure 7C** shows that this residue tends to be oriented toward the solvent. The interaction of hIAPP(H18+) with the membrane is dominated by K1, but the hydrophobic residues of the C-terminal side (F23, I26, and L27) can also insert into the membrane, yet without forming a helix. Alternatively, these three residues can form a hydrophobic cluster, which can give rise to a β-hairpin as seen for both hIAPP and hIAPP(H18+) (**Figure Figure5**).

3.5 The Peptides Have No Noteworthy Effects on the Membrane Properties

With polarized ATR-FTIR spectroscopy, not only the secondary structure of the peptides can be probed, also the effect of the peptides on the organization of the lipidic membrane can be determined. This is possible by measuring the position of the bands corresponding to antisymmetric and symmetric stretching modes of the methylene groups of the lipid tails, ν_{as} (CH_2) and ν_s (CH_2) in the absence and in the presence of the peptides as well as the dichroic ratio (R_{ATR}) of the ν_s (CH_2) bands (**Table 3**) (Goormaghtigh et al., 1999). The wavenumbers of these bands are known to be sensitive to changes in the configuration of the acyl chains, in chain mobility, and packing. For the bilayer alone, ν_s (CH_2) and ν_{as} (CH_2) are 2854 and 2945 cm^{-1}, respectively, and the value of R_{ATR} is 1.28, which is characteristic for fluid and packed acyl chains. The addition of hIAPP to the bilayer does not significantly change the wavenumbers, while there is a slight

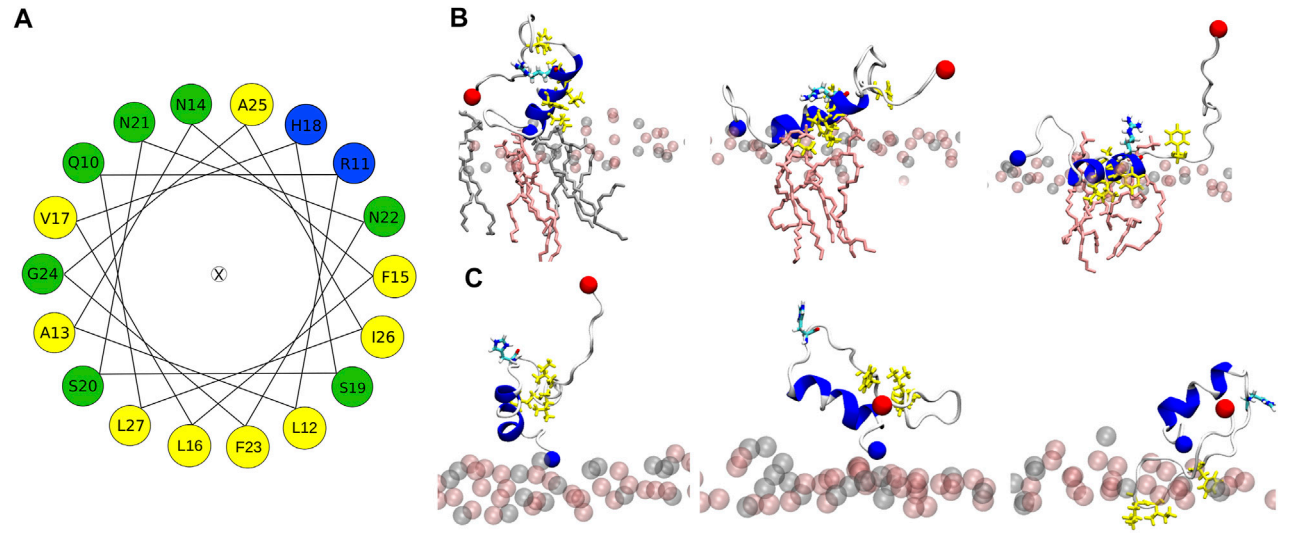

FIGURE 7 | (A) Helical wheel of residues Q10 to L27 of hIAPP. Hydrophobic residues are highlighted by yellow, positively charged ones by blue, and polar residues by green. The orientation of the wheel was chosen such that the residues that insert into the membrane are located at the bottom. **(B)** This situation can be seen for IAPP-H18R. The initial membrane association is driven by electrostatic interactions between K1 and the lipid headgroups (left). Next, the hydrophobic residues (side chains shown in yellow) start inserting (middle) until their side chains are within the hydrophobic membrane core (right). This interaction is further stabilized by H-bonds between R18 and the lipid headgroups. **(C)** In the case of hIAPP(H18+) the side chain is too short for stable interactions between this residue and the membrane. Instead, this interaction is dominated by K1 (left and middle) or the hydrophobic residues F23, I26, and L27, while being in a non-helical state, insert into the hydrohpobic membrane core (right). The lipid headgroups are shown as spheres and in **(B)** the lipid heads close to the peptide are shown as sticks.

TABLE 3 | Wavenumbers and dichroic ratio for the methylene groups of the lipid chains in the absence and presence of IAPP peptides.

	ν_{as} (CH_2) (cm^{-1})	ν_s (CH_2) (cm^{-1})	R_{ATR} (ν_s (CH_2))
Supported lipid bilayer	2924	2854	1.28 ± 0.07
+ hIAPP	2919	2851	1.34 ± 0.07
+ H18R-IAPP	2927	2855	1.29 ± 0.07
+ H18K-IAPP	2927	2855	1.27 ± 0.07
+ H18E-IAPP	2925	2854	1.26 ± 0.07
+ H18A-IAPP	2926	2855	1.20 ± 0.07

increase in R_{ATR} for the ν_s (CH_2) bands, which indicates a minor increase in disorder in the lipid chains. In contrast, in the presence of the mutated peptides, the wavenumbers are not modified, suggesting that these peptides do not or hardly affect the organization of the lipid bilayers. Thus, our results show that the mutated peptides do not alter the membrane properties during the first peptide–membrane interaction events, while hIAPP slightly increases the disorder in the membrane resulting from initial peptide insertions into the membrane.

This conclusion is supported by the analysis of the membrane bilayer properties from the MD simulations. From the mass density profiles of the DOPC and DOPS headgroups along the membrane *z*-axis we determined the average bilayer thickness as ≈ 4 nm. In order to assess whether the peptides affect the membrane properties, we analyzed the bilayer thickness around the membrane-associated peptides (**Supplementary Figure S4**). In these areas, reductions in the bilayer thickness of up to ≈0.1 nm are detected. However, hIAPP and H18A-IAPP have only small to no effects on the bilayer thickness, suggesting that a charged amino acid at position 18 plays a role in causing membrane perturbations, especially when it enables membrane insertion. This is best seen for H18R- and H18K-IAPP that triggered the largest changes in membrane thickness, which are the same two peptides that inserted into the membrane during the simulations. For further characterization of the membrane properties, we calculated the order parameter of the C–H bonds in the lipid acyl chains (denoted as S_{CH}) for both DOPC and DOPS lipids. Here, we distinguished between lipids that are in the vicinity of the peptides (i.e., within 0.5 nm) and all other lipids, to observe whether the peptides can cause lipid disorder (**Supplementary Figure S5**). Similar S_{CH} profiles along the acyl chains (characterized by carbon number) are observed for DOPC and DOPS, with the order parameters of the latter being slightly higher. A strong drop in order is present at the double bonds positioned at carbon atom 10 of both palmitoyl and oleoyl chains of either lipid type. Most importantly, no notable change in lipid order due to the presence of any of the peptides is observed. This suggests that changes to the lipid thickness resulted only from the interactions between the peptides and the lipid headgroups, while the acyl chains are not affected as none of the peptides did insert deeply into the membrane core, maximally just below the headgroup region in the cases of H18R- and H18K-IAPP. Apart from hIAPP this agrees to the observations from the experiments, as also there the lipid tail packing was not affected by the peptides, suggesting that also in the experiments the peptides did not penetrate into the

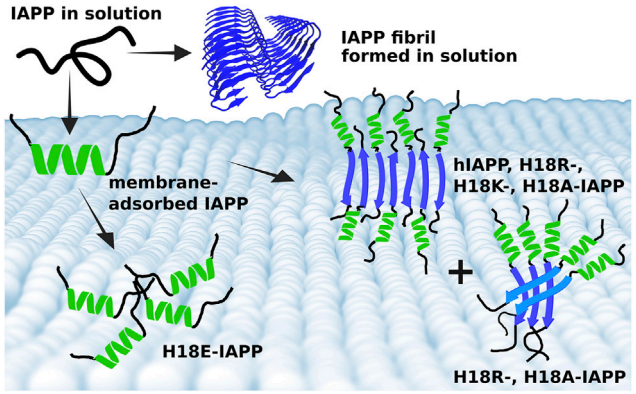

FIGURE 8 | Summary of the different IAPP-membrane interaction modes. (Top) In solution, IAPP is mainly intrinsically disordered and can aggregate into amyloid fibrils, which are characterized by parallel β-sheets (blue cartoon, produced from PDB entry 6Y1A (Röder et al., 2020). (Bottom) On the membrane, IAPP adopts initially a helix (green), which is of amphipathic nature and hence tethers the peptide to the membrane. Following membrane binding, the peptides start aggregating where the structure, and size of the aggregates depend on the nature of residue 18. Wild-type hIAPP as well as H18R-, H18K-, and H18A-IAPP form fibrils with antiparallel β-sheets. However, there is also some helix and random coil present in these fibrillar structures, suggesting that the N-terminal and membrane-bound helix remains, while residues from S20 onward form an antiparallel β-sheet. This arrangement allows the fibrils to grow. In the case of a parallel β-sheet, on the other hand, the helices are too close to each other for fibril formation to take place. Instead, oligomers which appear as amorphous aggregates are formed, as observed for H18R- and H18A-IAPP. In the case of H18E-IAPP, no β-sheet formation takes place. Instead, random coil and helix are the prevailing secondary structures.

membrane core. Only in the case of hIAPP some minor changes in the acyl packing were recorded, indicating that in the experiments this peptide was able to notably reach beyond the headgroup region. Interestingly, this is the same peptide that formed the largest amounts of (antiparallel) β-sheets, suggesting that β-sheet formation and membrane insertion take place concurrently.

4 CONCLUSION

In the present study, ATR-FTIR and TEM experiments as well as all-atom MD simulations on the microsecond time scale have been performed to unravel the first structural changes of the islet amyloid polypeptide following its interaction with a lipid membrane. Moreover, the influence of residue 18 in this process was assessed by studying wild-type hIAPP and variants of it with mutations H18A, H18E, H18K, and H18R.

The secondary structure profiles from simulations suggest that initially the membrane-bound IAPP is mostly in a random coil conformation (≈30–40%) with some α-helices. All mutants show higher amounts of helix than hIAPP, especially H18K-IAPP (≈45%) and H18A-IAPP (≈38%). While alanine is commonly known to be a helix-promoting amino acid, also lysine has a high helix-forming propensity. The notably lower amounts in β-sheet in the simulations compared to what is observed experimentally is due to the different length and time scales that are assessed. The simulations are limited to one peptide and one microsecond and, hence, focus on exploring the structural preferences of the IAPP monomers following membrane binding. On the time scale and with the temporal resolution of the experiments, on the other hand, peptide aggregation takes place to a certain extent; they therefore provide information on a changing mixture of monomers, oligomers and fibrils. The analysis of the ATR-FTIR spectra demonstrates that at the beginning of the experiments, the peptides are predominantly unstructured (35–50%) with contributions from α-helical structures (12% for H18E-IAPP and ≈20% for the other peptides) and β-sheets (12–35%). During the course of 2 h of incubation, the ATR-FTIR spectra of hIAPP revealed an increase in the antiparallel β-sheet content and a reduction in the α-helical and random coil contents, and which is in agreement with the TEM images that revealed fibrils with typical amyloid morphology. Similar data as for hIAPP were obtained for H18K-IAPP that also experienced an increase in anti-parallel β-sheet content and exhibited typical amyloid fibrils. For H18R-IAPP and H18A-IAPP, both the ATR-FTIR spectra and TEM images indicate the presence of two species, one of them being structured in antiparallel β-sheets, and the other one involving parallel β-sheets. The TEM images further revealed two different supramolecular structures, thin and short fibrils as well as amorphous aggregates. We propose that the fibrils are composed of the antiparallel β-sheets, as seen for hIAPP and H18K-IAPP, while the amorphous aggregates contain parallel β-sheets. In all four peptides, the formation of β-sheets was accompanied by reductions in random coil, which was especially the case for hIAPP. The reductions in α-helix content were minor, with the helical amount remaining at 15–20%. H18E-IAPP is the only peptide for which no transitions into β-sheets were observed, neither in the ATR-FTIR spectra nor did fibrils occur in the TEM images. Instead, the amount of helix increased with time.

Based on these observations we suggest an aggregation scheme of membrane-adsorbed IAPP peptides as summarized in **Figure 8**. Considering that the amount of helix remains almost constant, or even increases in the case of H18E-IAPP, we assume that the initial membrane-anchoring helix in the N-terminal half of the peptide is very stable and resists the transformation into β-sheets. The simulations revealed that for all peptide variants this helix is located between residues Q10 and S19, but it generally does not involve all of these ten residues as this would amount to a helical content of more than 27%. The β-sheet formation is thus expected to take place in the C-terminal peptide region from residue S20 onwards. For several fragments of that region it has been shown that amyloid-fibril formation is possible. This especially applies to the region S20–S29, which is also considered the amyloid-core region of hIAPP. Solid-state NMR spectroscopy (Griffiths et al., 1995) and X-ray crystallography of microcrystals formed by hexa- or heptapeptides from that region (PDB entries 3DG1, 3DGJ, 5E61, and 5E5V) (Wiltzius et al., 2008, 2009; Soriaga et al., 2016) showed that these segments can form both antiparallel and parallel β-sheets, while for the fibrils formed in solution by full-length IAPP (**Figure 8**), only parallel β-sheets have been

reported (Röder et al., 2020; Gallardo et al., 2020; Cao et al., 2020). We thus conclude that for membrane-bound IAPP, the decision whether parallel β-sheets are formed in addition to antiparallel ones depends on the characteristics of the membrane-bound helix involving residue 18. In the case of antiparallel β-sheets, the helices are far enough away from each other (see **Figure 8**) that the nature of residue 18 does almost not matter, as this structure is adopted for all peptides but H18E-IAPP. In the latter case, the electrostatic repulsion arising from the interplay of E18 and the negative membrane-surface charges prevents an alignment of the helices for β-sheet formation to take place. For the occurrence of parallel β-sheets, the helices need to get even closer, as **Figure 8** shows. Such an arrangement seems only be possible for A18 and R18. While the former is not surprising given its small volume and neutral charge, the latter is more remarkable, especially when considering its similarity with K18 that did not yield parallel β-sheets. However, Lys and Arg are known to interact differently with lipid membranes: Arg attracts more phosphate and water in the membrane, and can form extensive hydrogen bonding with its five H-bond donors that stabilize Arg-phosphate clusters (Li et al., 2013). This should lead to an effective charge screening between the neighbored helices of H18R-IAPP. Nonetheless, it should be noted that, at the current stage, this is a hypothesis, which will be tested by our future studies.

Previous reports revealed that hIAPP and H18K-IAPP are toxic to β-cell lines (Khemtemourian et al., 2017). Based on our current observations, we suggest that the toxic hIAPP and H18K-IAPP species are those that are structured with antiparallel β-sheets, as different behaviors are observed for the other peptides. In the case of hIAPP, the joint analysis of the experimental and simulation data suggests that the β-sheet aggregates even started to insert into the lipid bilayers, causing membrane disorder, and which would explain their toxicity. The absence of pronounced β-sheet formation in the case of H18E-IAPP concurs with the previous finding that this peptide is the least toxic H18 mutant (Khemtemourian et al., 2017) and reinforces our hypothesis that cytotoxicity and the presence of antiparallel β-sheet structures are correlated in IAPP. For other amyloid proteins such correlation has already been demonstrated. Using a yeast amyloid from the HET-s prion domain of *Podospora anserina*, Cullin and coworkers showed that mutations within the HET-s prion domain give rise to antiparallel β-sheet structures and, at the same time, enhance the cytotoxicity (Berthelot et al., 2011). Other toxic amyloid-forming proteins also adopt an antiparallel β-sheet conformation, such as the amyloid-β peptide involved in Alzheimer's disease, and α-synuclein related to Parkinson's disease (Cerf et al., 2009; Celej et al., 2012), suggesting that the antiparallel β-sheet is a signature of amyloid toxicity.

Earlier studies indicated that hIAPP and the mutated peptides are able to induce membrane permeability (Hoffmann et al., 2018a). Here, we tested for possible membrane disorder induced by the peptide using both ATR-FTIR and MD simulations. Consistent with previous MD studies, the peptides approach the membrane via their N-terminal residues (K1–R19) (Engel et al., 2006; Skeby et al., 2016). This interaction between peptide and membrane is mainly driven by electrostatic attractions between the positively charged residues K1 and R11 and the negatively charged lipid DOPS, which is strengthened when there is a third positive charge at position 18, as seen for H18K- and H18R-IAPP. However, hIAPP(H18+) did not interact more strongly with the membrane, suggesting that, in addition to the charge at residue 18, and also the size and/or flexibility of the side chain plays a role in affecting peptide–membrane interactions. In the simulations, the helical regions of H18K- and H18R-IAPP were able to insert into the membrane, adopting a parallel orientation with respect to the membrane surface where the hydrophobic side chains entered the hydrophobic membrane core and the hydrophilic side chains point in the opposite direction towards the aqueous phase. This orientation is stabilized by the long and flexible side chains of K1, R11, and K18 or R18. The ATR-FTIR results reflect that the mutated peptides H18R-, H18K-, H18E-, and H18A-IAPP do not alter the membrane properties during the initial peptide–membrane interactions, while hIAPP was able to slightly change the membrane properties. Since this is the peptide with the largest amount of β-sheets being formed, this suggests that β-sheets are needed for membrane disturbances. This conjecture is further supported by our MD data which revealed that the initial insertion of IAPP as a helix is only just below the headgroup region, which, apart from small effects on the membrane thickness around the peptide, does not change the lipid tail order. This agrees to the findings from the ATR-FTIR spectra. Hence, we conclude that apart from hIAPP, no deep insertions of the peptides into the membrane occurred in the current experiments. Various membrane damage mechanisms caused by hIAPP have been proposed and described in detail, which implicate the presence of large oligomers or fibrils and involve pore formation or lipid uptake (Engel, 2009). Our experimental and simulation results indicate that the initial IAPP aggregate species are not able to inflict such membrane destabilization.

In summary, the results of this study provide valuable molecular level insight into understanding of the initial IAPP–membrane interactions and demonstrate how mutations at residue 18 can affect this interaction and fibril formation of IAPP (**Figure 8**). We demonstrated that a single mutation of histidine 18 can yield vastly different results in terms aggregate morphology, membrane damage, and resulting toxicity, highlighting once again the importance of this residue in amyloid formation by hIAPP.

DATA AVAILABILITY STATEMENT

The original contributions presented in the study are included in the article/**Supplementary Material**, further inquiries can be directed to the corresponding authors.

AUTHOR CONTRIBUTIONS

LK designed the study. LK performed the TEM and analyzed the images. LK and BD performed the ATR-FTIR experiments; LK, SL, and SC analyzed the ATR-FTIR spectra. HF and BS designed the computer simulations. HF performed the simulations and analyzed them together with BS. LK, HF, and BS wrote the manuscript. All authors contributed to discussing the results and reviewing the manuscript.

FUNDING

HF and BS acknowledge funding for this project from the Palestinian-German Science Bridge financed by the German Federal Ministry of Education and Research.

ACKNOWLEDGMENTS

Christophe Piesse (Institut de Biologie Paris Seine, Université Pierre et Marie Curie, France) is acknowledged for the peptides synthesis. HF and BS gratefully acknowledge the computing time granted through JARA on the supercomputer JURECA at Forschungszentrum Jülich (project number JICS6C).

SUPPLEMENTARY MATERIAL

The Supplementary Material for this article can be found online at: https://www.frontiersin.org/articles/10.3389/fmolb.2022.849979/full#supplementary-material

REFERENCES

Abedini, A., and Raleigh, D. P. (2009). A Critical Assessment of the Role of Helical Intermediates in Amyloid Formation by Natively Unfolded Proteins and Polypeptides. *Protein Eng. Des. Selection* 22, 453–459. doi:10.1093/protein/gzp036

Abedini, A., and Raleigh, D. P. (2006). Destabilization of Human Iapp Amyloid Fibrils by Proline Mutations outside of the Putative Amyloidogenic Domain: Is There a Critical Amyloidogenic Domain in Human Iapp? *J. Mol. Biol.* 355, 274–281. doi:10.1016/j.jmb.2005.10.052

Abraham, M. J., Murtola, T., Schulz, R., Páll, S., Smith, J. C., Hess, B., et al. (2015). GROMACS: High Performance Molecular Simulations through Multi-Level Parallelism from Laptops to Supercomputers. *SoftwareX* 1-2, 19–25. doi:10.1016/j.softx.2015.06.001

Berendsen, H. J. C., Postma, J. P. M., van Gunsteren, W. F., DiNola, A., and Haak, J. R. (1984). Molecular Dynamics with Coupling to an External bath. *J. Chem. Phys.* 81, 3684–3690. doi:10.1063/1.448118

Berthelot, K., Ta, H. P., Géan, J., Lecomte, S., and Cullin, C. (2011). *In Vivo* and *In Vitro* Analyses of Toxic Mutants of Het-S: Ftir Antiparallel Signature Correlates with Amyloid Toxicity. *J. Mol. Biol.* 412, 137–152. doi:10.1016/j.jmb.2011.07.009

Brender, J. R., Hartman, K., Reid, K. R., Kennedy, R. T., and Ramamoorthy, A. (2008a). A Single Mutation in the Nonamyloidogenic Region of Islet Amyloid Polypeptide Greatly Reduces Toxicity. *Biochemistry* 47, 12680–12688. doi:10.1021/bi801427c

Brender, J. R., Lee, E. L., Cavitt, M. A., Gafni, A., Steel, D. G., and Ramamoorthy, A. (2008b). Amyloid Fiber Formation and Membrane Disruption Are Separate Processes Localized in Two Distinct Regions of Iapp, the Type-2-Diabetes-Related Peptide. *J. Am. Chem. Soc.* 130, 6424–6429. doi:10.1021/ja710484d

Bussi, G., Donadio, D., and Parrinello, M. (2007). Canonical Sampling through Velocity Rescaling. *J. Chem. Phys.* 126, 014101. doi:10.1063/1.2408420

Caillon, L., Hoffmann, A. R. F., Botz, A., and Khemtemourian, L. (20162016). Molecular Structure, Membrane Interactions, and Toxicity of the Islet Amyloid Polypeptide in Type 2 Diabetes Mellitus. *J. Diabetes Res.* 2016, 1–13. doi:10.1155/2016/5639875:

Caillon, L., Lequin, O., and Khemtémourian, L. (2013). Evaluation of Membrane Models and Their Composition for Islet Amyloid Polypeptide-Membrane Aggregation. *Biochim. Biophys. Acta (Bba) - Biomembranes* 1828, 2091–2098. doi:10.1016/j.bbamem.2013.05.014

Cao, P., Marek, P., Noor, H., Patsalo, V., Tu, L.-H., Wang, H., et al. (2013). Islet Amyloid: From Fundamental Biophysics to Mechanisms of Cytotoxicity. *FEBS Lett.* 587, 1106–1118. doi:10.1016/j.febslet.2013.01.046

Cao, Q., Boyer, D. R., Sawaya, M. R., Ge, P., and Eisenberg, D. S. (2020). Cryo-em Structure and Inhibitor Design of Human Iapp (Amylin) Fibrils. *Nat. Struct. Mol. Biol.* 27, 653–659. doi:10.1038/s41594-020-0435-3

Celej, M. S., Sarroukh, R., Goormaghtigh, E., Fidelio, G. D., Ruysschaert, J.-M., and Raussens, V. (2012). Toxic Prefibrillar α-synuclein Amyloid Oligomers Adopt a Distinctive Antiparallel β-sheet Structure. *Biochem. J.* 443, 719–726. doi:10.1042/bj20111924

Cerf, E., Sarroukh, R., Tamamizu-Kato, S., Breydo, L., Derclaye, S., Dufrêne, Y. F., et al. (2009). Antiparallel β-sheet: a Signature Structure of the Oligomeric Amyloid β-peptide. *Biochem. J.* 421, 415–423. doi:10.1042/bj20090379

Choi, B., Kim, N. H., Jin, G. Y., Kim, Y. S., Kim, Y. H., and Eom, K. (2021). Sequence-dependent Aggregation-Prone Conformations of Islet Amyloid Polypeptide. *Phys. Chem. Chem. Phys.* 23, 22532–22542. doi:10.1039/D1CP01061A

Christensen, M., Berglund, N. A., and Schiøtt, B. (2021). The Effect of Cholesterol on Membrane-Bound Islet Amyloid Polypeptide. *Front. Mol. Biosci.* 8, 657946. doi:10.3389/fmolb.2021.657946

Cooper, G. J., Willis, A. C., Clark, A., Turner, R. C., Sim, R. B., and Reid, K. B. (1987). Purification and Characterization of a Peptide from Amyloid-Rich Pancreases of Type 2 Diabetic Patients. *Proc. Natl. Acad. Sci.* 84, 8628–8632. doi:10.1073/pnas.84.23.8628

de Koning, E. J. P., Fleming, K. A., Gray, D. W. R., and Clark, A. (1995). High Prevalence of Pancreatic Islet Amyloid in Patients with End-Stage Renal Failure on Dialysis Treatment. *J. Pathol.* 175, 253–258. doi:10.1002/path.1711750214

Despa, S., Margulies, K. B., Chen, L., Knowlton, A. A., Havel, P. J., Taegtmeyer, H., et al. (2012). Hyperamylinemia Contributes to Cardiac Dysfunction in Obesity and Diabetes. *Circ. Res.* 110, 598–608. doi:10.1161/circresaha.111.258285

Dignon, G. L., Zerze, G. H., and Mittal, J. (2017a). Interplay between Membrane Composition and Structural Stability of Membrane-Bound Hiapp. *J. Phys. Chem. B* 121, 8661–8668. doi:10.1021/acs.jpcb.7b05689

Dignon, G. L., Zerze, G. H., and Mittal, J. (2017b). Interplay between Membrane Composition and Structural Stability of Membrane-Bound hIAPP. *J. Phys. Chem. B* 121, 8661–8668. doi:10.1021/acs.jpcb.7b05689

Dong, X., Qiao, Q., Qian, Z., and Wei, G. (2018). Recent Computational Studies of Membrane Interaction and Disruption of Human Islet Amyloid Polypeptide: Monomers, Oligomers and Protofibrils. *Biochim. Biophys. Acta (Bba) - Biomembranes* 1860, 1826–1839. doi:10.1016/j.bbamem.2018.03.006

Engel, M. F. M., Khemtemourian, L., Kleijer, C. C., Meeldijk, H. J. D., Jacobs, J., Verkleij, A. J., et al. (2008). Membrane Damage by Human Islet Amyloid Polypeptide through Fibril Growth at the Membrane. *Proc. Natl. Acad. Sci.* 105, 6033–6038. doi:10.1073/pnas.0708354105

Engel, M. F. M. (2009). Membrane Permeabilization by Islet Amyloid Polypeptide. *Chem. Phys. Lipids* 160, 1–10. doi:10.1016/j.chemphyslip.2009.03.008

Engel, M. F. M., Yigittop, H., Elgersma, R. C., Rijkers, D. T. S., Liskamp, R. M. J., de Kruijff, B., et al. (2006). Islet Amyloid Polypeptide Inserts into Phospholipid Monolayers as Monomer. *J. Mol. Biol.* 356, 783–789. doi:10.1016/j.jmb.2005.12.020

Evers, F., Jeworrek, C., Tiemeyer, S., Weise, K., Sellin, D., Paulus, M., et al. (2009). Elucidating the Mechanism of Lipid Membrane-Induced Iapp Fibrillogenesis and its Inhibition by the Red Wine Compound Resveratrol: A Synchrotron

X-ray Reflectivity Study. *J. Am. Chem. Soc.* 131, 9516–9521. doi:10.1021/ja8097417

Fox, A., Snollaerts, T., Errecart Casanova, C., Calciano, A., Nogaj, L. A., and Moffet, D. A. (2010). Selection for Nonamyloidogenic Mutants of Islet Amyloid Polypeptide (IAPP) Identifies an Extended Region for Amyloidogenicity. *Biochemistry* 49, 7783–7789. doi:10.1021/bi100337p

Gallardo, R., Iadanza, M. G., Xu, Y., Heath, G. R., Foster, R., Radford, S. E., et al. (2020). Fibril Structures of Diabetes-Related Amylin Variants Reveal a Basis for Surface-Templated Assembly. *Nat. Struct. Mol. Biol.* 27, 1048–1056. doi:10.1038/s41594-020-0496-3

Gao, M., and Winter, R. (2015). The Effects of Lipid Membranes, Crowding and Osmolytes on the Aggregation, and Fibrillation Propensity of Human Iapp. *J. Diabetes Res.* 2015, 1–21. doi:10.1155/2015/849017

Goldsbury, C., Goldie, K., Pellaud, J., Seelig, J., Frey, P., Müller, S. A., et al. (2000). Amyloid Fibril Formation from Full-Length and Fragments of Amylin. *J. Struct. Biol.* 130, 352–362. doi:10.1006/jsbi.2000.4268

Goormaghtigh, E., Cabiaux, V., and Ruysschaert, J.-M. (1994). Determination of Soluble and Membrane Protein Structure by Fourier Transform Infrared Spectroscopy. *Physicochemical methods in the study of biomembranes*, 405–450. doi:10.1007/978-1-4615-1863-1_10

Goormaghtigh, E., Cabiaux, V., and Ruysschaert, J.-M. (1990). Secondary Structure and Dosage of Soluble and Membrane Proteins by Attenuated Total Reflection Fourier-Transform Infrared Spectroscopy on Hydrated Films. *Eur. J. Biochem.* 193, 409–420. doi:10.1111/j.1432-1033.1990.tb19354.x

Goormaghtigh, E., Raussens, V., and Ruysschaert, J.-M. (1999). Attenuated Total Reflection Infrared Spectroscopy of Proteins and Lipids in Biological Membranes. *Biochim. Biophys. Acta (Bba) - Rev. Biomembranes* 1422, 105–185. doi:10.1016/s0304-4157(99)00004-0

Griffiths, J. M., Ashburn, T. T., Auger, M., Costa, P. R., Griffin, R. G., and Lansbury, P. T., Jr (1995). Rotational Resonance Solid-State Nmr Elucidates a Structural Model of Pancreatic Amyloid. *J. Am. Chem. Soc.* 117, 3539–3546. doi:10.1021/ja00117a023

Hebda, J. A., and Miranker, A. D. (2009). The Interplay of Catalysis and Toxicity by Amyloid Intermediates on Lipid Bilayers: Insights from Type Ii Diabetes. *Annu. Rev. Biophys.* 38, 125–152. doi:10.1146/annurev.biophys.050708.133622

Hess, B., Bekker, H., Berendsen, H. J. C., and Fraaije, J. G. E. M. (1997). Lincs: a Linear Constraint Solver for Molecular Simulations. *J. Comput. Chem.* 18, 1463–1472. doi:10.1002/(sici)1096-987x(199709)18:12<1463:aid-jcc4>3.0.co;2-h

Hoffmann, A. R. F., Caillon, L., Salazar Vazquez, L. S., Spath, P.-A., Carlier, L., Khemtémourian, L., et al. (2018b). Time Dependence of NMR Observables Reveals Salient Differences in the Accumulation of Early Aggregated Species between Human Islet Amyloid Polypeptide and Amyloid-β. *Phys. Chem. Chem. Phys.* 20, 9561–9573. doi:10.1039/C7CP07516B

Hoffmann, A. R. F., Saravanan, M. S., Lequin, O., Killian, J. A., and Khemtemourian, L. (2018a). A Single Mutation on the Human Amyloid Polypeptide Modulates Fibril Growth and Affects the Mechanism of Amyloid-Induced Membrane Damage. *Biochim. Biophys. Acta (Bba) - Biomembranes* 1860, 1783–1792. doi:10.1016/j.bbamem.2018.02.018

Höppener, J. W. M., Ahrén, B., and Lips, C. J. M. (2000). Islet Amyloid and Type 2 Diabetes Mellitus. *N. Engl. J. Med.* 343, 411–419. doi:10.1056/NEJM200008103430607

Huang, J., Rauscher, S., Nawrocki, G., Ran, T., Feig, M., de Groot, B. L., et al. (2017). CHARMM36m: an Improved Force Field for Folded and Intrinsically Disordered Proteins. *Nat. Methods* 14, 71–73. doi:10.1038/nmeth.4067

Janson, J., Ashley, R. H., Harrison, D., McIntyre, S., and Butler, P. C. (1999). The Mechanism of Islet Amyloid Polypeptide Toxicity Is Membrane Disruption by Intermediate-Sized Toxic Amyloid Particles. *Diabetes* 48, 491–498. doi:10.2337/diabetes.48.3.491

Jayasinghe, S. A., and Langen, R. (2005). Lipid Membranes Modulate the Structure of Islet Amyloid Polypeptide. *Biochemistry* 44, 12113–12119. doi:10.1021/bi050840w

Jorgensen, W. L., Chandrasekhar, J., Madura, J. D., Impey, R. W., and Klein, M. L. (1983). Comparison of Simple Potential Functions for Simulating Liquid Water. *J. Chem. Phys.* 79, 926–935. doi:10.1063/1.445869

Kabsch, W., and Sander, C. (1983). Dictionary of Protein Secondary Structure: Pattern Recognition of Hydrogen-Bonded and Geometrical Features. *Biopolymers* 22, 2577–2637. doi:10.1002/bip.360221211

Kayed, R., Sokolov, Y., Edmonds, B., McIntire, T. M., Milton, S. C., Hall, J. E., et al. (2004). Permeabilization of Lipid Bilayers Is a Common Conformation-dependent Activity of Soluble Amyloid Oligomers in Protein Misfolding Diseases. *J. Biol. Chem.* 279, 46363–46366. doi:10.1074/jbc.C400260200

Khemtemourian, L., Antoniciello, F., Sahoo, B. R., Decossas, M., Lecomte, S., and Ramamoorthy, A. (2021). Investigation of the Effects of Two Major Secretory Granules Components, Insulin and Zinc, on Human-Iapp Amyloid Aggregation and Membrane Damage. *Chem. Phys. Lipids* 237, 105083. doi:10.1016/j.chemphyslip.2021.105083

Khemtémourian, L., Engel, M. F. M., Liskamp, R. M. J., Höppener, J. W. M., and Killian, J. A. (2010). The N-Terminal Fragment of Human Islet Amyloid Polypeptide Is Non-fibrillogenic in the Presence of Membranes and Does Not Cause Leakage of Bilayers of Physiologically Relevant Lipid Composition. *Biochim. Biophys. Acta (Bba) - Biomembranes* 1798, 1805–1811. doi:10.1016/j.bbamem.2010.05.022

Khemtemourian, L., Guillemain, G., Foufelle, F., and Killian, J. A. (2017). Residue Specific Effects of Human Islet Polypeptide Amyloid on Self-Assembly and on Cell Toxicity. *Biochimie* 142, 22–30. doi:10.1016/j.biochi.2017.07.015

Klauda, J. B., Venable, R. M., Freites, J. A., O'Connor, J. W., Tobias, D. J., Mondragon-Ramirez, C., et al. (2010). Update of the CHARMM All-Atom Additive Force Field for Lipids: Validation on Six Lipid Types. *J. Phys. Chem. B* 114, 7830–7843. doi:10.1021/jp101759q

Knowles, T. P. J., Vendruscolo, M., and Dobson, C. M. (2014). The Amyloid State and its Association with Protein Misfolding Diseases. *Nat. Rev. Mol. Cel Biol.* 15, 384–396. doi:10.1038/nrm3810

Lee, J., Cheng, X., Swails, J. M., Yeom, M. S., Eastman, P. K., Lemkul, J. A., et al. (2016). CHARMM-GUI Input Generator for NAMD, GROMACS, AMBER, OpenMM, and CHARMM/OpenMM Simulations Using the CHARMM36 Additive Force Field. *J. Chem. Theor. Comput.* 12, 405–413. doi:10.1021/acs.jctc.5b00935

Li, L., Vorobyov, I., and Allen, T. W. (2013). The Different Interactions of Lysine and Arginine Side Chains with Lipid Membranes. *J. Phys. Chem. B* 117, 11906–11920. doi:10.1021/jp405418y

Ling, Y. L., Strasfeld, D. B., Shim, S.-H., Raleigh, D. P., and Zanni, M. T. (2009). Two-dimensional Infrared Spectroscopy Provides Evidence of an Intermediate in the Membrane-Catalyzed Assembly of Diabetic Amyloid. *J. Phys. Chem. B* 113, 2498–2505. doi:10.1021/jp810261x

Liu, Y., Zhang, D., Zhang, Y., Tang, Y., Xu, L., He, H., et al. (2020). Molecular Dynamics Simulations of Cholesterol Effects on the Interaction of Hiapp with Lipid Bilayer. *J. Phys. Chem. B* 124, 7830–7841. doi:10.1021/acs.jpcb.0c05742

Lutz, T. A. (2010). The Role of Amylin in the Control of Energy Homeostasis. *Am. J. Physiology-Regulatory, Integr. Comp. Physiol.* 298, R1475–R1484. doi:10.1152/ajpregu.00703.2009

Martel, A., Antony, L., Gerelli, Y., Porcar, L., Fluitt, A., Hoffmann, K., et al. (2016). Membrane Permeation versus Amyloidogenicity: A Multitechnique Study of Islet Amyloid Polypeptide Interaction with Model Membranes. *J. Am. Chem. Soc.* 139, 137–148. doi:10.1021/jacs.6b06985

Mei, L., Shen, W., Wu, X., Liu, J., Li, D., and Ji, B. (2020). Interactions of Human Islet Amyloid Polypeptide with Lipid Structure of Different Curvatures. *Theor. Appl. Mech. Lett.* 10, 412–418. doi:10.1016/j.taml.2020.01.053

Milardi, D., Gazit, E., Radford, S. E., Xu, Y., Gallardo, R. U., Caflisch, A., et al. (2021). Proteostasis of Islet Amyloid Polypeptide: a Molecular Perspective of Risk Factors and Protective Strategies for Type Ii Diabetes. *Chem. Rev.* 121, 1845–1893. doi:10.1021/acs.chemrev.0c00981

Miller, Y. (2022). Advancements and Future Directions in Research of the Roles of Insulin in Amyloid Diseases. *Biophysical Chem.* 281, 106720. doi:10.1016/j.bpc.2021.106720

Mirzabekov, T. A., Lin, M.-C., and Kagan, B. L. (1996). Pore Formation by the Cytotoxic Islet Amyloid Peptide Amylin. *J. Biol. Chem.* 271, 1988–1992. doi:10.1074/jbc.271.4.1988

Mishra, R., Bulic, B., Sellin, D., Jha, S., Waldmann, H., and Winter, R. (2008). Small-molecule Inhibitors of Islet Amyloid Polypeptide Fibril Formation. *Angew. Chem.* 120, 4757–4760. doi:10.1002/ange.200705372

Mishra, R., and Winter, R. (2008). Cold- and Pressure-Induced Dissociation of Protein Aggregates and Amyloid Fibrils. *Angew. Chem. Int. Ed.* 47, 6518–6521. doi:10.1002/anie.200802027

Nanga, R. P. R., Brender, J. R., Vivekanandan, S., and Ramamoorthy, A. (2011). Structure and Membrane Orientation of Iapp in its Natively Amidated Form at

Physiological Ph in a Membrane Environment. *Biochim. Biophys. Acta (Bba) - Biomembranes* 1808, 2337–2342. doi:10.1016/j.bbamem.2011.06.012

Nguyen, P. H., Ramamoorthy, A., Sahoo, B. R., Zheng, J., Faller, P., Straub, J. E., et al. (2021). Amyloid Oligomers: A Joint Experimental/Computational Perspective on Alzheimer's Disease, Parkinson's Disease, Type II Diabetes, and Amyotrophic Lateral Sclerosis. *Chem. Rev.* 121, 2545–2647. doi:10.1021/acs.chemrev.0c01122

Opie, E. L. (1901). The Relation Oe Diabetes Mellitus to Lesions of the Pancreas. Hyaline Degeneration of the Islands Oe Langerhans. *J. Exp. Med.* 5, 527–540. doi:10.1084/jem.5.5.527

Patil, S. M., Xu, S., Sheftic, S. R., and Alexandrescu, A. T. (2009). Dynamic α-Helix Structure of Micelle-Bound Human Amylin. *J. Biol. Chem.* 284, 11982–11991. doi:10.1074/jbc.m809085200

Poojari, C., Xiao, D., Batista, V. S., and Strodel, B. (2013). Membrane Permeation Induced by Aggregates of Human Islet Amyloid Polypeptides. *Biophysical J.* 105, 2323–2332. doi:10.1016/j.bpj.2013.09.045

Press-Sandler, O., and Miller, Y. (2018). Molecular Mechanisms of Membrane-Associated Amyloid Aggregation: Computational Perspective and Challenges. *Biochim. Biophys. Acta (Bba) - Biomembranes* 1860, 1889–1905. doi:10.1016/j.bbamem.2018.03.014

Qian, Z., Zou, Y., Zhang, Q., Chen, P., Ma, B., Wei, G., et al. (2018). Atomistic-level Study of the Interactions between Hiapp Protofibrils and Membranes: Influence of Ph and Lipid Composition. *Biochim. Biophys. Acta (Bba) - Biomembranes* 1860, 1818–1825. doi:10.1016/j.bbamem.2018.02.005

Qiao, Q., Wei, G., Yao, D., and Song, Z. (2019). Formation of α-helical and β-sheet Structures in Membrane-Bound Human IAPP Monomer and the Resulting Membrane Deformation. *Phys. Chem. Chem. Phys.* 21, 20239–20251. doi:10.1039/c9cp03151k

Quist, A., Doudevski, I., Lin, H., Azimova, R., Ng, D., Frangione, B., et al. (2005). Amyloid Ion Channels: A Common Structural Link for Protein-Misfolding Disease. *Proc. Natl. Acad. Sci.* 102, 10427–10432. doi:10.1073/pnas.0502066102

Radovan, D., Smirnovas, V., and Winter, R. (2008). Effect of Pressure on Islet Amyloid Polypeptide Aggregation: Revealing the Polymorphic Nature of the Fibrillation Process. *Biochemistry* 47, 6352–6360. doi:10.1021/bi800503j

Röder, C., Kupreichyk, T., Gremer, L., Schäfer, L. U., Pothula, K. R., Ravelli, R. B. G., et al. (2020). Cryo-EM Structure of Islet Amyloid Polypeptide Fibrils Reveals Similarities with Amyloid-β Fibrils. *Nat. Struct. Mol. Biol.* 27, 660–667. doi:10.1038/s41594-020-0442-4

Rodriguez Camargo, D. C., Tripsianes, K., Buday, K., Franko, A., Göbl, C., Hartlmüller, C., et al. (2017). The Redox Environment Triggers Conformational Changes and Aggregation of hIAPP in Type II Diabetes. *Sci. Rep.* 7, 44041. doi:10.1038/srep44041

Rouser, G., Fleischer, S., and Yamamoto, A. (1970). Two Dimensional Thin Layer Chromatographic Separation of Polar Lipids and Determination of Phospholipids by Phosphorus Analysis of Spots. *Lipids* 5, 494–496. doi:10.1007/bf02531316

Rustenbeck, I., Matthies, A., and Lenzen, S. (1994). Lipid Composition of Glucose-Stimulated Pancreatic Islets and Insulin-Secreting Tumor Cells. *Lipids* 29, 685–692. doi:10.1007/bf02538912

Seeliger, J., Weise, K., Opitz, N., and Winter, R. (2012). The Effect of Aβ on IAPP Aggregation in the Presence of an Isolated β-Cell Membrane. *J. Mol. Biol.* 421, 348–363. doi:10.1016/j.jmb.2012.01.048

Selkoe, D. J. (2004). Erratum: Folding Proteins in Fatal Ways. *Nature* 428, 445. doi:10.1038/nature02477

Sepehri, A., Nepal, B., and Lazaridis, T. (2021). Distinct Modes of Action of Iapp Oligomers on Membranes. *J. Chem. Inf. Model.* 61, 4645–4655. doi:10.1021/acs.jcim.1c00767

Skeby, K. K., Andersen, O. J., Pogorelov, T. V., Tajkhorshid, E., and Schiøtt, B. (2016). Conformational Dynamics of the Human Islet Amyloid Polypeptide in a Membrane Environment: Toward the Aggregation Prone Form. *Biochemistry* 55, 2031–2042. doi:10.1021/acs.biochem.5b00507

Soriaga, A. B., Sangwan, S., Macdonald, R., Sawaya, M. R., and Eisenberg, D. (2016). Crystal Structures of Iapp Amyloidogenic Segments Reveal a Novel Packing Motif of Out-Of-Register Beta Sheets. *J. Phys. Chem. B* 120, 5810–5816. doi:10.1021/acs.jpcb.5b09981

Sparr, E., Engel, M. F. M., Sakharov, D. V., Sprong, M., Jacobs, J., de Kruijff, B., et al. (2004). Islet Amyloid Polypeptide-Induced Membrane Leakage Involves Uptake of Lipids by Forming Amyloid Fibers. *FEBS Lett.* 577, 117–120. doi:10.1016/j.febslet.2004.09.075

Srodulski, S., Sharma, S., Bachstetter, A. B., Brelsfoard, J. M., Pascual, C., Xie, X. S., et al. (2014). Neuroinflammation and Neurologic Deficits in Diabetes Linked to Brain Accumulation of Amylin. *Mol. Neurodegeneration* 9, 30. doi:10.1186/1750-1326-9-30

Tu, L.-H., and Raleigh, D. P. (2013). Role of Aromatic Interactions in Amyloid Formation by Islet Amyloid Polypeptide. *Biochemistry* 52, 333–342. doi:10.1021/bi3014278

Westermark, P., Andersson, A., and Westermark, G. T. (2011). Islet Amyloid Polypeptide, Islet Amyloid, and Diabetes Mellitus. *Physiol. Rev.* 91, 795–826. doi:10.1152/physrev.00042.2009

Westermark, P., Wernstedt, C., Wilander, E., Hayden, D. W., O'Brien, T. D., and Johnson, K. H. (1987). Amyloid Fibrils in Human Insulinoma and Islets of Langerhans of the Diabetic Cat Are Derived from a Neuropeptide-like Protein Also Present in normal Islet Cells. *Proc. Natl. Acad. Sci.* 84, 3881–3885. doi:10.1073/pnas.84.11.3881

Willbold, D., Strodel, B., Schröder, G. F., Hoyer, W., and Heise, H. (2021). Amyloid-type Protein Aggregation and Prion-like Properties of Amyloids. *Chem. Rev.* 121, 8285–8307. doi:10.1021/acs.chemrev.1c00196

Williamson, J. A., and Miranker, A. D. (2007). Direct Detection of Transient α-helical States in Islet Amyloid Polypeptide. *Protein Sci.* 16, 110–117. doi:10.1110/ps.062486907

Wiltzius, J. J. W., Sievers, S. A., Sawaya, M. R., Cascio, D., Popov, D., Riekel, C., et al. (2008). Atomic Structure of the Cross-β Spine of Islet Amyloid Polypeptide (Amylin). *Protein Sci.* 17, 1467–1474. doi:10.1110/ps.036509.108

Wiltzius, J. J. W., Sievers, S. A., Sawaya, M. R., and Eisenberg, D. (2009). Atomic Structures of Iapp (Amylin) Fusions Suggest a Mechanism for Fibrillation and the Role of Insulin in the Process. *Protein Sci.* 18, 1521–1530. doi:10.1002/pro.145

Wineman-Fisher, V., and Miller, Y. (2016). Effect of Zn2+ Ions on the Assembly of Amylin Oligomers: Insight into the Molecular Mechanisms. *Phys. Chem. Chem. Phys.* 18, 21590–21599. doi:10.1039/C6CP04105A

Zhang, X., St. Clair, J. R. J. R., London, E., and Raleigh, D. P. (2017). Islet Amyloid Polypeptide Membrane Interactions: Effects of Membrane Composition. *Biochemistry* 56, 376–390. doi:10.1021/acs.biochem.6b01016

Zhang, Y., Luo, Y., Deng, Y., Mu, Y., and Wei, G. (2012). Lipid Interaction and Membrane Perturbation of Human Islet Amyloid Polypeptide Monomer and Dimer by Molecular Dynamics Simulations. *PLOS ONE* 7, e38191. doi:10.1371/journal.pone.0038191

Conflict of Interest: The authors declare that the research was conducted in the absence of any commercial or financial relationships that could be construed as a potential conflict of interest.

Publisher's Note: All claims expressed in this article are solely those of the authors and do not necessarily represent those of their affiliated organizations, or those of the publisher, the editors and the reviewers. Any product that may be evaluated in this article, or claim that may be made by its manufacturer, is not guaranteed or endorsed by the publisher.